JOURNAL OF GEOPHYSICAL RESEARCH, VOL. 106, NO. C8, PAGES 16,603–16,622, AUGUST 15, 2001

A comparison of surface eddy kinetic energy and Reynolds stresses in the Gulf Stream and the Kuroshio Current systems from merged TOPEX/Poseidon and ERS-1/2 altimetric data

N. Ducet and P.-Y. Le Traon

Space Oceanography Division, Collecte Localisation Satellite, Toulouse, France

Abstract. Analyses of surface eddy kinetic energy (EKE) inferred from 5 years of merged TOPEX/Poseidon and ERS-1/2 altimetric data are presented in the Gulf Stream (GS) and the Kuroshio (KS) Current systems, focusing on anisotropy and EKE seasonal, interannual, and long-term variations, as well as Reynolds stresses. For both GS and KS a descriptive analysis of the EKE field shows that it is anisotropic along the path of the currents and assesses the close relationship between the spatial distribution of EKE high levels and bottom topography. A striking ocean feature is found in the GS, shaped as a zonal "double-blade" structure in the EKE field, centered at 37°N, 71.5°W, that likely corresponds to a regular and permanent lateral displacement of the mean path of the current at this geographical location. Maps of EKE seasonal means for years 1993, 1996, and 1997 provide a detailed description of the surface variability (meanders, pinched-off eddies, etc.) and show strong interannual variations in the KS. EKE monthly mean changes in the KS reveal a well-marked seasonal cycle during the first 3 years (1993–1995), with EKE peaking in July/August. This is followed by a constant increase of its level, from the beginning of year 1996 till the beginning of 1997. During this increase the zonal velocity variance $<u'^2>$ is up to 30% higher than its meridional counterpart, suggesting a zonal acceleration of the eastward flow. EKE seasonal changes are also found in the KS Current (30°–35°N, 130°–140°E) and also show a regular annual cycle during the first 3 years, which precedes by 2 months the EKE seasonal cycle in the KS Extension (maximum in May/June). The maximum in EKE in both regions precedes by 2 months the maximum surface transport found by *Qiu et al.* [1991] and *Zlotnicki* [1991], occurring in July and late September, respectively. No such annual cycle is found in the GS region during the first 3 years. Year 1996 is anomalous in both current systems, with mean EKE level that increases by more than 20% compared to the other years. Also, EKE monthly mean changes in the KS reveal a well-marked positive tendency in the eastern part of the current of more than 300 $cm^2\ s^{-2}\ yr^{-1}$ and a negative tendency both in its eastern part and in the KS Current. This feature is absent from the GS. At last, eddy/mean flow interaction is presented. Both the spatial averaging of turbulent quantities and the relative contribution of the different terms of the horizontal momentum fluxes are discussed. A tentative explanation is given for the anomalously large $<u'^2>$ at the end of 1996 in the KS Extension.

1. Introduction

The Gulf Stream (GS) and the Kuroshio (KS) Current systems are among the most energetic current systems in the world ocean and are dominant features of the North Atlantic and North Pacific circulation, respectively. After separating from the western boundaries at Cape Hatteras and Tokara Strait both the GS and the KS flow into the deep ocean, where they are characterized as eastward flowing jets associated by large-amplitude meanders and pinched-off eddies. Description and understanding of the dynamics of these currents, the associated mesoscale eddies, and their interactions with the large-scale circulation are fundamental to improving our understanding of the ocean general circulation.

Paper number 2000JC000205.
0148-02277/01/2000JC000205$09.00

Satellite altimetry provides a unique opportunity to study sea level and ocean circulation changes with a high accuracy and a space/time sampling suitable for monitoring mesoscale to large-scale signals. Many previous works on the two western boundary current systems have used altimeter data [e.g., *Tai and White*, 1990; *Kelly*, 1991; *Zlotnicki*, 1991; *Qiu*, 1992, 1995; *Wang and Koblinsky*, 1995, 1999; *Wang et al.*, 1998; *Adamec*, 1998] to study the energetics (meanders, eddies, Reynolds stresses, etc.) of these currents, the seasonal cycle of their surface transport, and the spatial structure and temporal fluctuations of their mesoscale variability.

These studies generally use along-track single satellite data, mainly Geosat and TOPEX/Poseidon (T/P). However, it is now generally admitted that to access a more complete description of the whole spectrum of the ocean surface variability, and, in particular, the mesoscale, the merging of altimeter data from at least two different missions is needed [*Le Traon*

and Dibarboure, 1999]. Furthermore, with along-track data from a single satellite, anisotropy analyses of the geostrophic velocity field are not possible, except at crossover points, because only the cross-track velocity can then be obtained. Therefore velocity and subsequent eddy kinetic energy (EKE) calculations have to be computed assuming isotropy.

This work is a regional extension of the global study on the contribution of the "optimal" merging of T/P and ERS data to the global mesoscale circulation [*Ducet et al.*, 2000] (here-inafter referred to as DLTR00). DLTR00 show that the combined maps allow them to give a very detailed description of the global surface EKE, retaining the same accuracy as for T/P but with a finer spatial resolution. They show that the merged data provide a better estimation of the meridional velocity and observe about 30% more energy than T/P data only. A comparison with surface drifters in the North Atlantic further reveals a very good agreement in the spatial structure and the energy level of the variability observed by the drifters and the merged altimeter data.

This analysis focuses on the GS and the KS Current systems, using the same combined map data set as in the above mentioned global study. Rather than solving a particular issue, this work aims at showing the use of the merged data set for mesoscale variability studies and reveals a high accuracy, presumably never achieved so far, for describing new ocean features and studying anisotropy of the velocity field. Maps of EKE are used, to discuss and compare the spatial distribution of the mesoscale variability in the current systems and examine the local anisotropy of the geostrophic velocity field. This allows us to describe new regional oceanographic features as well. Time variations of the EKE are then analyzed ranging from the seasonal to interannual and pluriannual frequencies. Eddy/mean flow interactions, focusing on horizontal eddy momentum fluxes and their influence on the mean flows, are finally presented.

The paper is organized as follows. The data, data processing, and objective analysis method are briefly described in section 2. The general and mean features of the surface EKE field are discussed in section 3. In particular, the anisotropy of the velocity field is discussed. A somewhat new oceanographic feature in the GS is also highlighted. Seasonal, interannual, and pluriannual fluctuations of the EKE field are analyzed in section 4. Eddy/mean flow interactions are discussed in section 5 and a summary of the results is given in section 6.

2. Data and Mapping

Five and a half years of T/P reprocessed merged Geophysical Data Records (GDR) and ERS-1/2 ocean products (OPRs) are used. The data span the period from the beginning of October 1992 to mid-May 1998. This corresponds to 207 full 10 day repeat cycles (from cycle 2 to 208) for T/P but only to 4 years and 3 months of ERS-1/2 35 day repeat cycle mission data. The missing ERS-1 period corresponds to the 168 day repeat cycle geodetic mission from December 24, 1993, to March 24, 1995.

T/P and ERS-1/2 sea surface height (SSH) data sets are first homogenized and intercalibrated [*Le Traon and Ogor*, 1998]. Along-track sea level anomalies (SLA) relative to a 3 year mean profile (1993–1995) are then obtained from a conventional repeat track analysis. To reduce measurement noise and mapping computer time, the SLA files are subsequently filtered and subsampled, as described by DLTR00.

The mapping of the ocean signal is done globally through an improved objective analysis method that takes long wavelength residual errors into account and uses realistic correlation scales of the ocean circulation. The reader is referred to DLTR00 for a detailed description of the mapping methodology. The space correlation scale (zero crossing of the correlation function) at 40°N, near the mean axes of both GS and KS, is 140 km, and the *e*-folding timescale is 15 days. Note that these scales are the ones corresponding to the global analysis and thus were not optimized for this regional mesoscale variability analysis.

SLA maps from October 1992 to May 1998 are used in this study for both T/P data only and the combination of T/P and ERS-1/2 data. There is one map every 10 days, and the grid resolution is 0.25° in latitude and longitude. T/P-only maps will only be used in section 4 when analyzing monthly mean EKE time series. Although less accurate than the combined maps, the T/P time series are continuous in time over the whole 5.5 year period.

3. Main EKE Features

In this section, differences between the GS and the KS Current systems are presented by describing general statistical characteristics, comparing EKE, $<u'^2>$, and $<v'^2>$ spatial distributions.

3.1. Kuroshio

Plate 1 shows the spatial distribution of the EKE, zonal $<u'^2>$, and meridional $<v'^2>$ velocity variances over the 5 year period. One can first note the band of the velocity variances higher than 2000 $cm^2\ s^{-2}$ in the KS Extension, which extends over about 20° in longitude, from 137° to 157°E at the Shatsky Rise. The width of this band is rather irregular, extending to 5° at 145°E and decreasing to about 1.5° at 155°E, associated with a slight southeastward deflection of the EKE envelope east of 150°E. The mesoscale variance, through the distribution of values of EKE, has a significant change along the axis of the KS, which suggests that the mean flow along the KS axis also has a similar variation [see, e.g., *Mizuno and White*, 1983].

One characteristic structure of the KS is the high EKE spot located south of Japan, between 135°E and 140°E, around 32°N, which is clearly identified in Plate 1b, where zonal eddy velocities are dominant. This offshore meander, south of Honshu, is detected in both altimeter and thermal (advanced very high resolution radiometer (AVHRR)) data [*Adamec*, 1998, Plate 1a]. It corresponds to a cold water mass that develops between the southern coast of Japan's Honshu island and a great southward meander of the KS before its path separates from the Japanese coast and becomes the KS Extension. For theoretical discussion on the bimodality of the KS and its different paths the reader is referred to *Chao* [1984] and *Kawabe* [1985; 1996]. This Kuroshio meander, as well as the two lee wave meanders centered at 144° and 150°E in the KS Extension at 35°N, are evident in the relative distribution of eddy velocity components (see Plates 1b and 1c). In combination with the meander that usually develops around 32°N, 158°E over the Shatsky Rise and which can extend southward down to 29°N (see section 4.1.1), they form the quasi-stationary meander pattern of the mean KS [*Mizuno and White*, 1983; *Qiu*, 1995], which is also well reproduced in a high-resolution simulation of the North Pacific Ocean [*Mitchell et al.*, 1996]. The spatial distribution of both components of the velocity variance

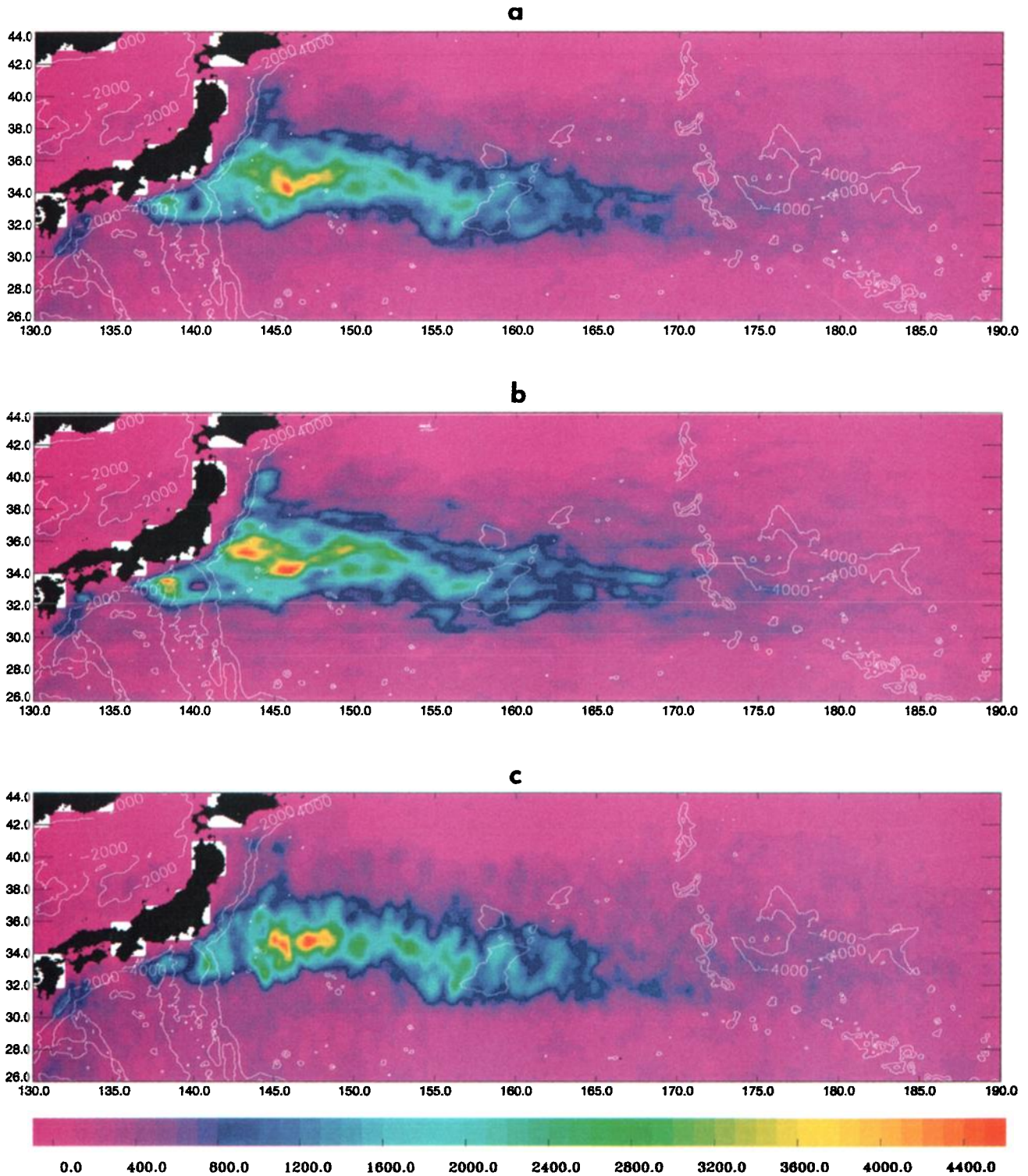

Plate 1. One-quarter degree resolution combined maps of (a) EKE, (b) $<u'^2>$, and (c) $<v'^2>$ in the KS Current system. Overlaid are the 2000 and 4000 m isobaths. Units are $cm^2\ s^{-2}$.

along the path of the current (Plates 1b and 1c) is then strongly anisotropic.

Plate 1a also shows that the maximum of EKE, more than 4500 $cm^2\ s^{-2}$, is found in a region around 146°E, 35°N, in between the two quasi-stationary meanders previously mentioned, where the maximum of the mean surface height differences across the KS Extension also occurs [*Qiu*, 1991]. Following *Nishida and White* [1982], this location also corresponds to the maximum peak of the mean kinetic energy, thus supporting the general belief that eddies are produced in the vicinity of strong currents through instability processes.

One can also infer from Plate 1 the close relationship between the EKE zonal distribution and the bottom topography. In the KS Current the maximum south of Honshu, at about

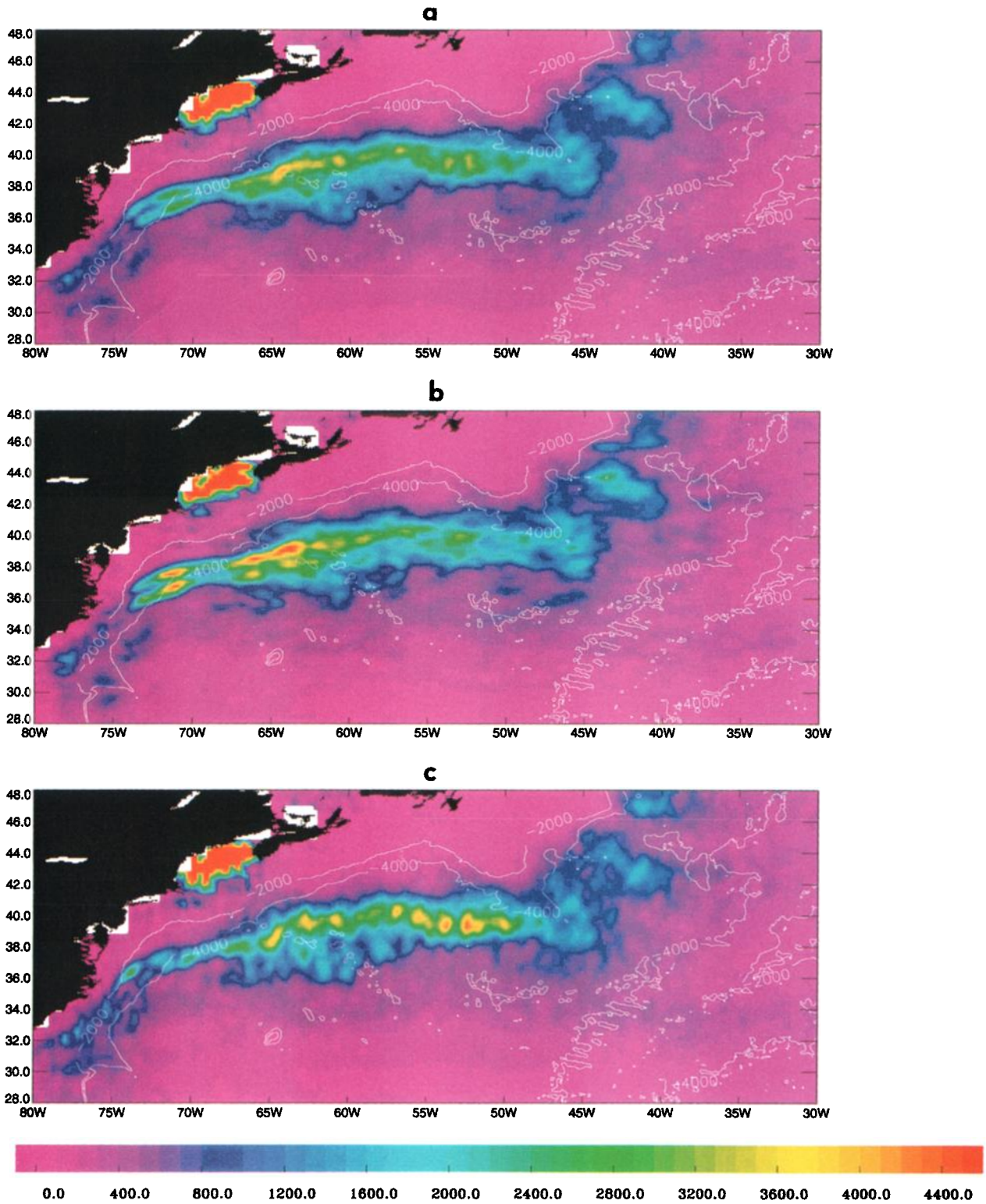

Plate 2. Same as Plate 1 but in the GS Current system.

139°E, 33°N, occurs between the 2000 and 4000 m isobath levels where bottom topography gradients are sharp. Besides, high-EKE values larger than 2000 $cm^2\ s^{-2}$ diminish abruptly at the location of the Shatsky Rise around 158°E, $<v'^2>$ being higher than $<u'^2>$ just west of it. Note that the modeling of *Hurlburt et al.* [1996] also indicates that some of the meandering features of the KS are due to the bathymetric influence of the seamounts (in particular, at 144°E).

3.2. Gulf Stream

The GS EKE spatial distribution is shown in Plate 2a. Contrary to what is observed in the KS area, high EKE values are more

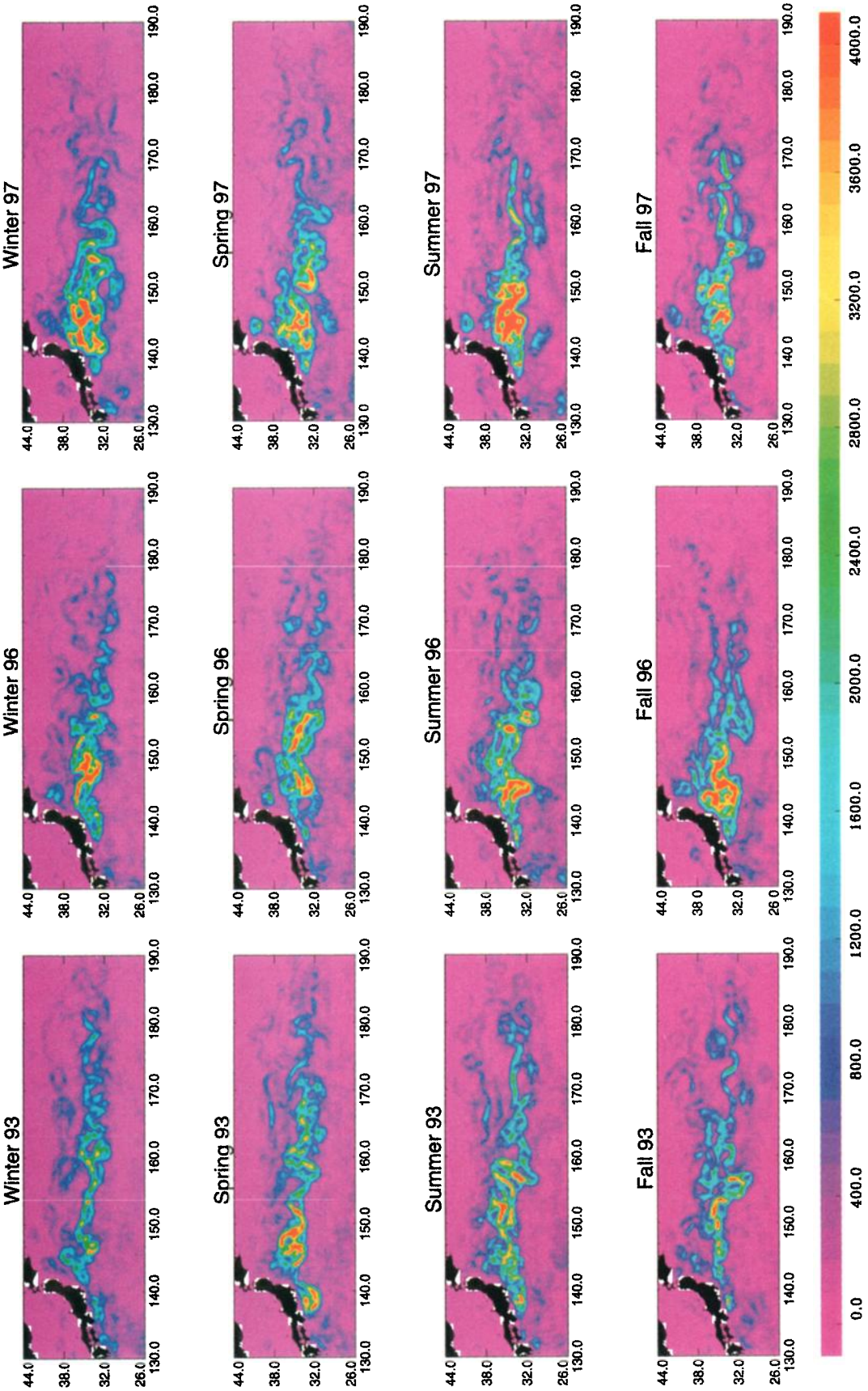

Plate 3. The EKE seasonal mean, inferred from the T/P + ERS−1/2 maps in the KS region, for years 1993, 1996, and 1997. The 2000 and 4000 m isobaths are overplotted. Units are in $cm^2\ s^{-2}$.

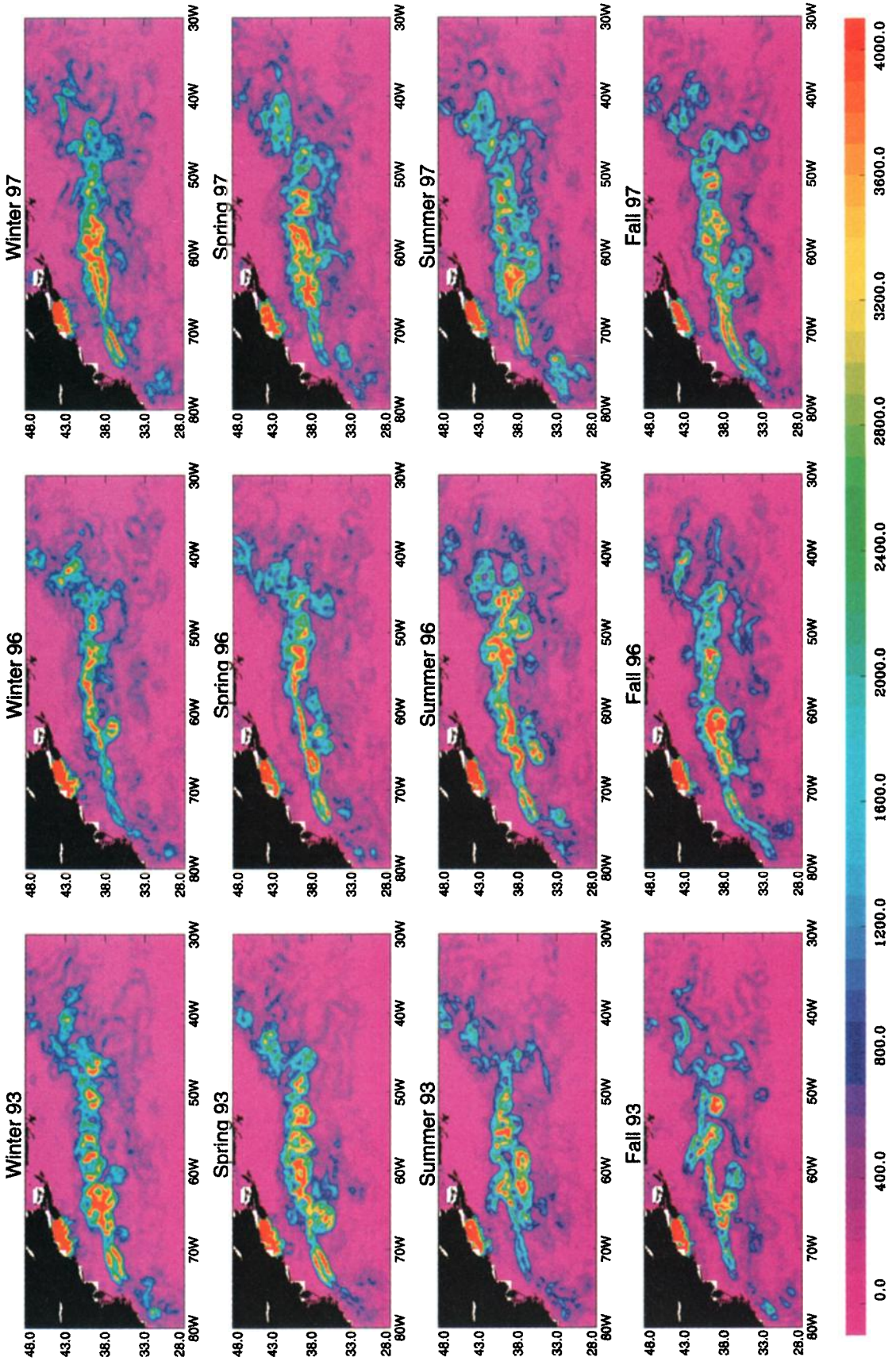

Plate 4. Same as Plate 3 but in the GS area.

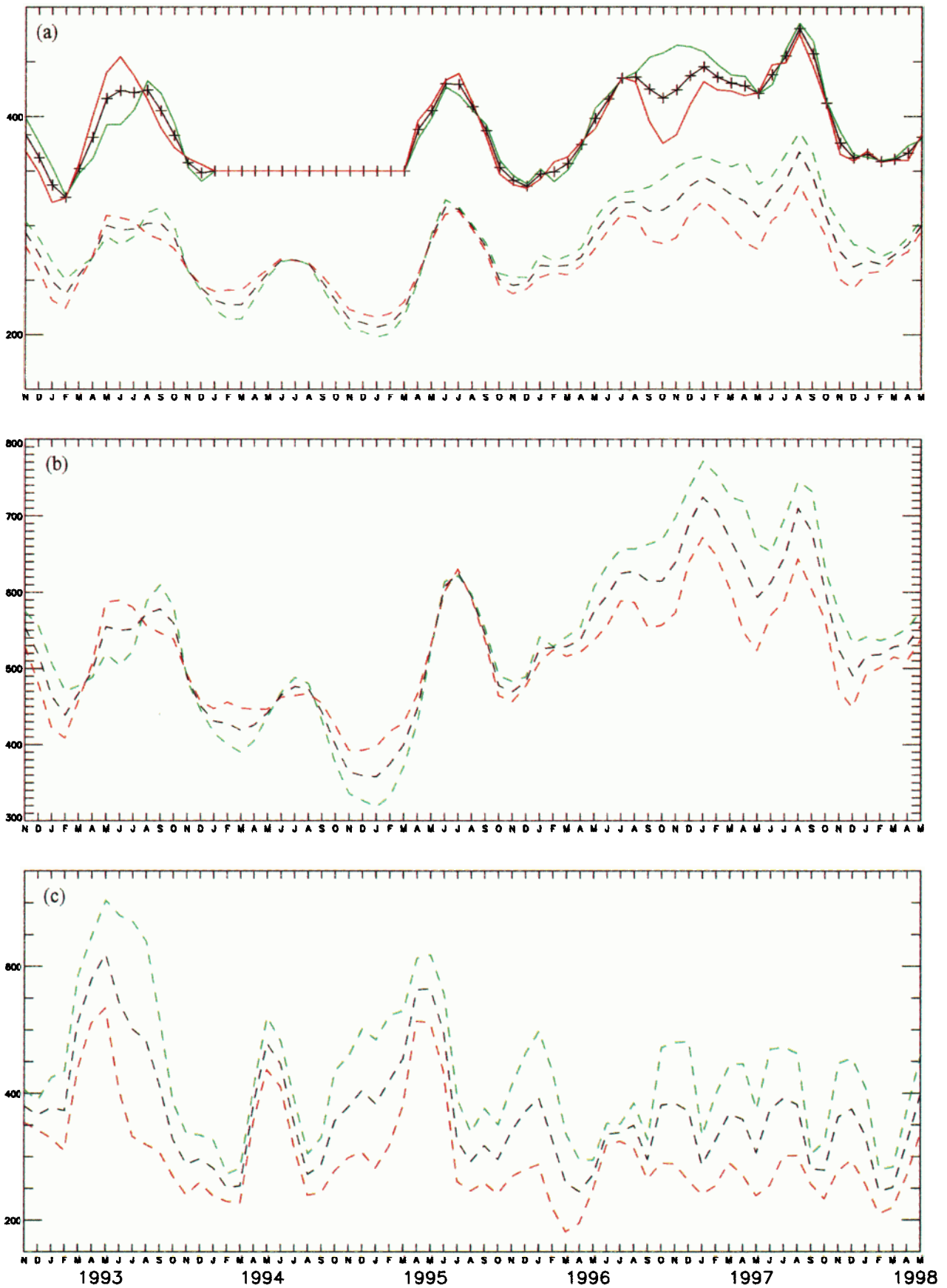

Plate 5. Time series of monthly mean EKE inferred from T/P and T/P + ERS− 1/2 maps in the the KS current system, defined as (a) 26°–44°N, 130°E–170°W, (b) 30°–40°, 140°–180°E (KS Extension), and (c) 30°–35°N, 130°–140°E (KS Current). Estimates are given for EKE (black), $\langle u'^2 \rangle$ (green), and $\langle v'^2 \rangle$ (orange), for T/P (dotted) and TP + ERS− 1/2 (solid). In Plates 5b and 5c, T/P-only data are used. EKE estimates are smoothed by a 3 month running mean (see text).

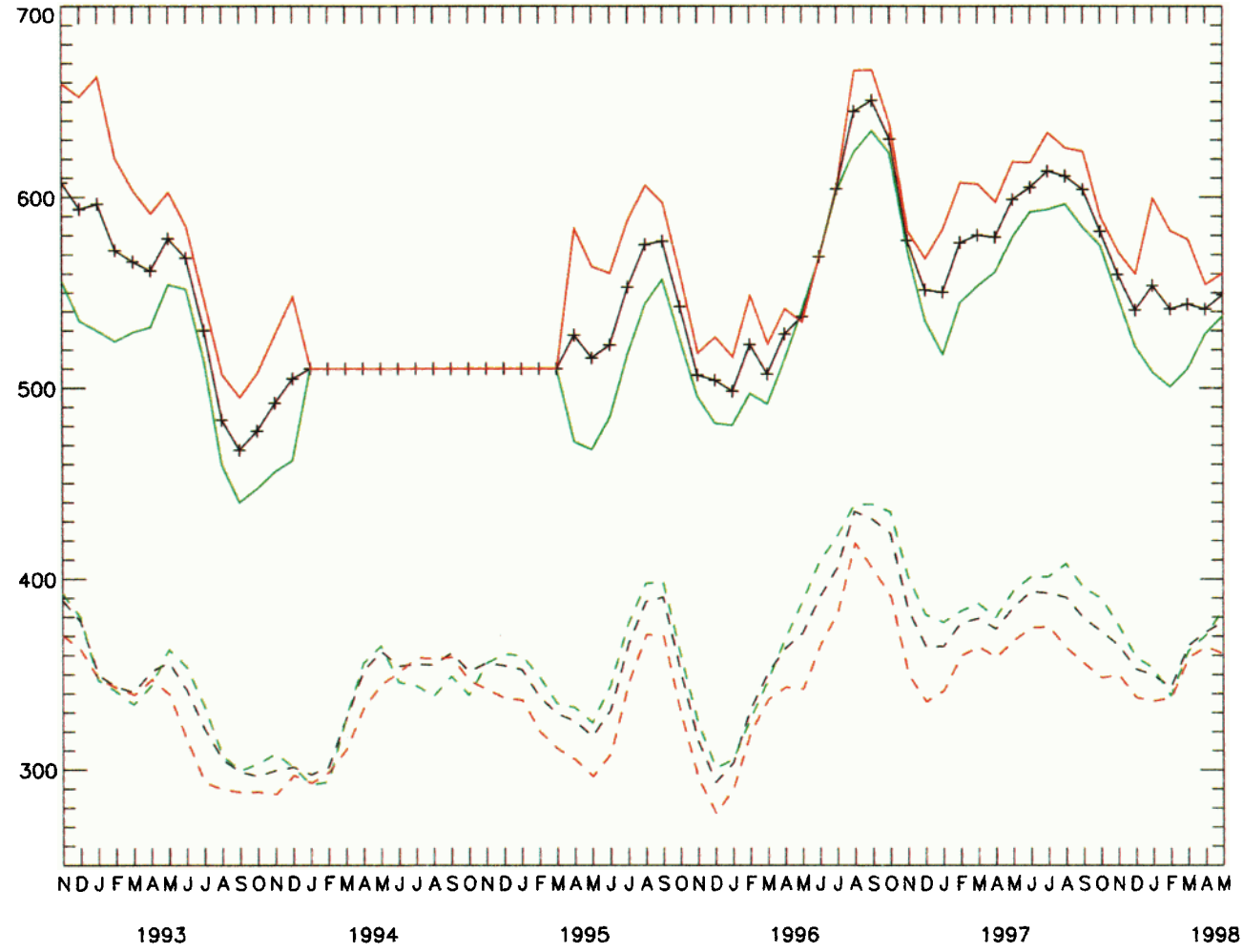

Plate 6. Same as Plate 5, but in the GS region defined as 28°–48°N, 80°–30°W.

tightly tied to the mean axis; that is, the mesoscale variance decreases more quickly away from the axis of the current than in the KS. The region of velocity variance higher than 2000 cm^2 s^{-2} is a rather narrow, zonal band that extends over 30° in longitude, from about 75° to 45°W. The width of this band is almost constant along the current path, about 3°, slightly larger at the New England Seamount Chain (NESC). Note that the large coastal anomaly at about 43°N, 68°W, in the bay of Fundy, does not represent any realistic ocean signal and is due to residual tidal errors (F. Lyard, personal communication, 1999).

Unlike the situation in the KS region, there is no significant lateral meandering after the current separates from the coast. Besides, the maximum in EKE is attained well downstream of coastal separation at Cape Hatteras, near 64°W, consistent with *Hall*'s [1991] results, whereas it occurs roughly 5° away from the Japanese coast in the KS.

The current system shows two different regimes, on each side of the NESC, at 64°–62°W. West of about 65°W, almost all the EKE results from the zonal velocity variance in a narrow band of high variability in which the meandering activity is low. One of the most striking and permanent feature of the eddy flow is a "double-blade" quasi-zonal structure, centered at 37°N, 71.5°W, just downstream of the current separation from the coast off Cape Hatteras (see Plate 2b). It corresponds to a very high SLA variability (more than 50 cm rms over the period) at the location where the current crosses the 4000 m isobath and starts flowing zonally. The flow here is strongly anisotropic, the zonal velocity variance being up to 3 times higher than the meridional one. The most likely cause for this oceanographic feature is a regular and permanent lateral displacement of the mean path of the GS current, with little meandering activity. *Tracey and Watts* [1986], in their 3 year analysis of the GS path fluctuations downstream of Cape Hatteras, computed histograms of its most northern wall locations along four cross-stream sections. They showed that by 72.5°W the GS was found with equal probability throughout its 145 km excursion range and could shift equally north to south, which corresponds well to the developed pattern. Nevertheless, the cause of such lateral displacements remains unclear. The location of this feature roughly corresponds to the crossing point between the Gulf Stream and the Deep Western Boundary Current (DWBC), so that one can wonder if there is any vertical shear influence of the DWBC on the GS path fluctuations. However, *Pickart*'s [1994] study on the interaction of the GS and the DWBC reveals that the DWBC simply responds to changing conditions in the GS instead of causing such changes, as suggested by earlier modeling studies.

Kelly [1991] discusses a significant anomaly in the surface transport near 69°W, where the width of the current also sig-

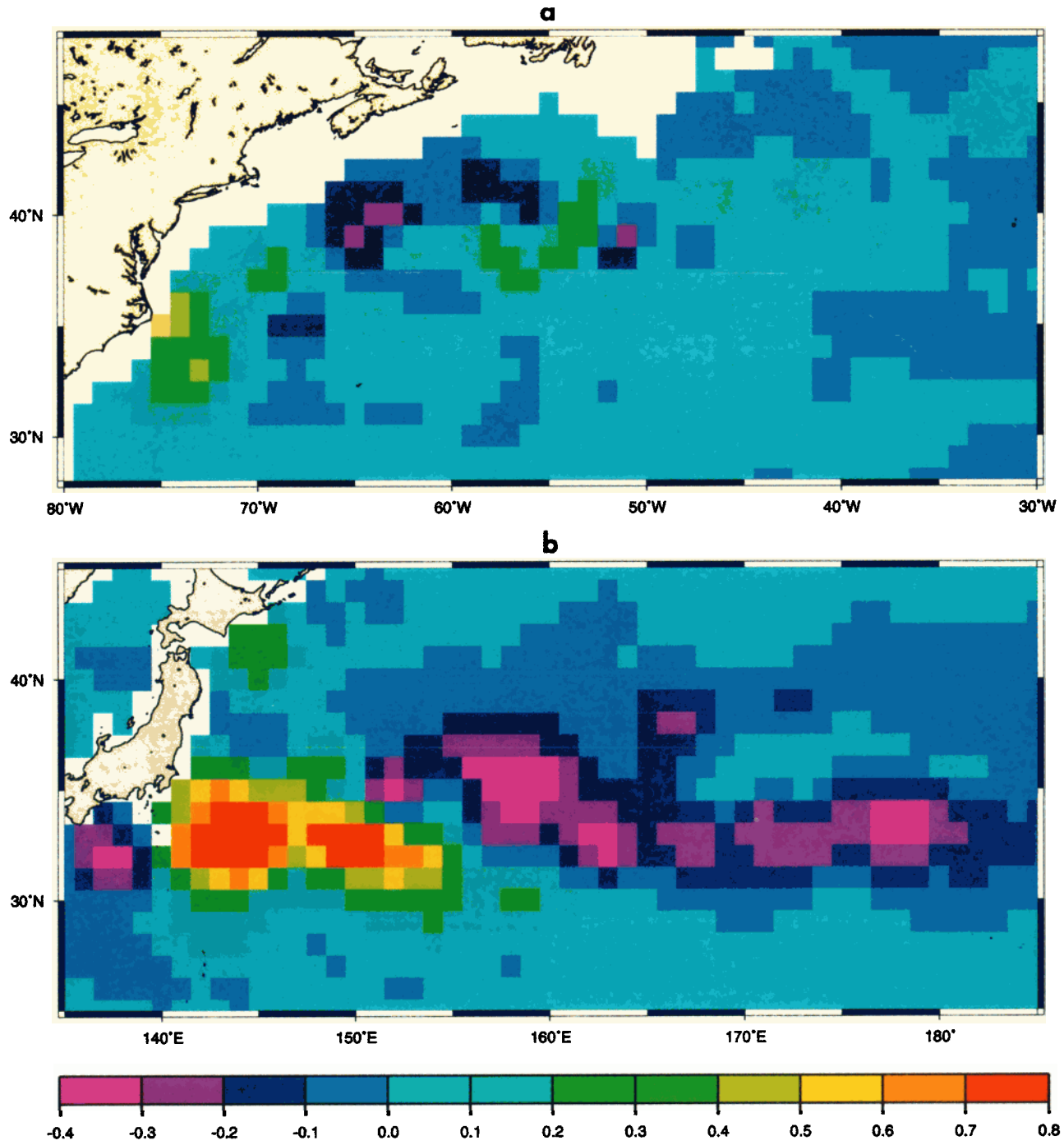

Plate 7. Linear trend in the monthly mean EKE field over the 5.5 year period, in $cm^2\ s^{-2}\ d^{-1}$ for (a) the GS and (b) the KS Current systems.

nificantly decreases, and suggests the existence of small-scale recirculation gyres there as an explanation. Her study also reveals a minimum in position variance of the mean axis of the GS around that location. Note that this minimum of the standard deviation of the GS envelope normal to the mean path of the current at about 70°W was also observed by *Cornillon* [1985] from satellite IR imagery. This minimum is also found in the EKE spatial distribution, inside a narrow channel of lower EKE values, generally smaller than 2000 $cm^2\ s^{-2}$.

East of 62°W, there is a strong and rapid decrease of zonal velocity variance with a significant increase of its meridional counterpart that reaches its maximum at about 52°W (Plate 2c), associated with a presumably much higher meandering activity and separated eddies. Note, again, that this relative spatial distribution of eddy velocity components is strongly anisotropic.

The correlation between high EKE level spatial distribution and bathymetry is evident in Plate 2, as was found for the KS. Examples include the double-blade location where the current separates from the coast at Cape Hatteras and flows over the 4000 m isobath; at 65°W, where the flow has a tendency to bifurcate on each side of the NESC; and at the southwestward

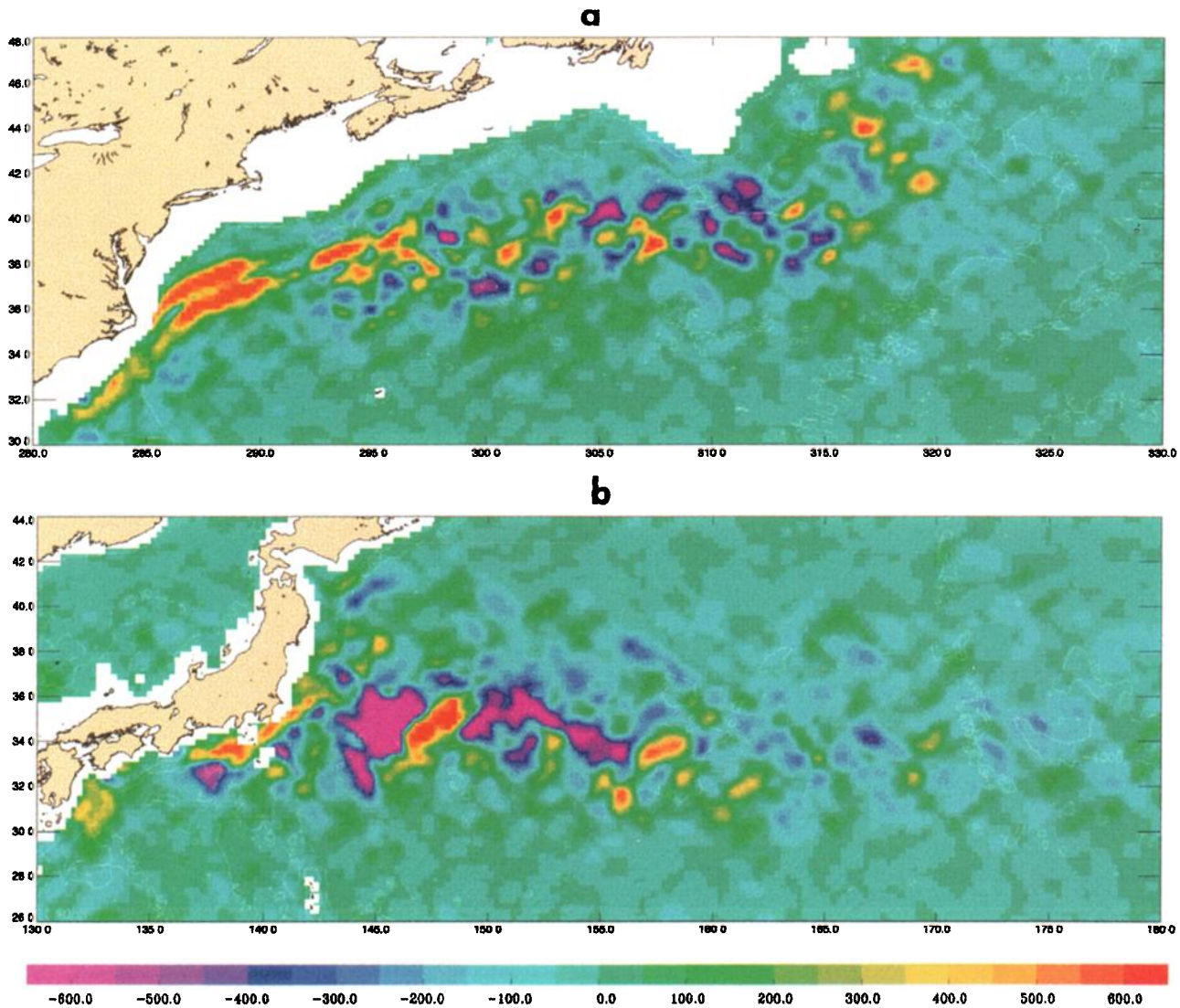

Plate 8. Reynolds stress cross-covariance term $<u'v'>$ for (a) the GS and (b) the KS Current systems. One-quarter degree resolution maps from October 1992 to December 1993 and from March 1995 to October 1997 are used. Units are $cm^2\ s^{-2}$.

incursion of the 4000 m isobath, down to 40°N, 47°W, which seems to create a southwestward deviation of the high EKE level envelope.

4. Seasonal and Interannual Variations of Mesoscale Variability

4.1. Time Fluctuations of EKE Spatial Distribution

4.1.1. Kuroshio. The variability of the KS Current is well developed in spring 1993 with lower values in 1996 and 1997 (Plate 3). The two meanders, centered at 144° and 150°E, can be observed in most seasons, particularly in winter and spring 1993 and summer 1996. The meander that forms at the Shatsky Rise is also clearly observed in fall 1993 and winter 1997, extending southward down to 29°N. Year 1993 exhibits rather seasonal oscillations in the intensity of the EKE, which is maximum in spring/summer and minimum in winter/fall, which will be confirmed in section 4.2.1. It is remarkable how quiescent the winter of year 1993 is, compared to, for example, the one of 1997. Years 1996 and 1997 do not show any clear seasonal variability in the EKE field but rather reveal strong interannual variations. Indeed, all the well-known energetic patterns mentioned above, particularly well observed in winter 1993, appear to be modified significantly during 1997: EKE levels can reach up to 10,000 $cm^2\ s^{-2}$ during summer 1997, the most energetic period, doubling the values of 1993. The envelope of high EKE levels is also much wider in 1997. This high EKE level is mainly associated with much stronger meandering activity and also terminates more abruptly zonally. For instance, considering the location around 180°E, 35°N, there is considerable energy in each season of 1993, on the order of 1500 $cm^2\ s^{-2}$, whereas the EKE level during 1997 is much lower. The zonal extension of the high EKE level is thus shorter and wider during 1997, reflecting strong interannual changes over the area. However, southward deflected meanders at the location of the Shatsky Rise are still present and likely correspond to the persistent influence of bottom topography. Also, note the presence of this pinched-off eddy pattern, situated at 41°N, 144°E, particularly well observed during spring and summer 1997 but also present throughout 1996. It

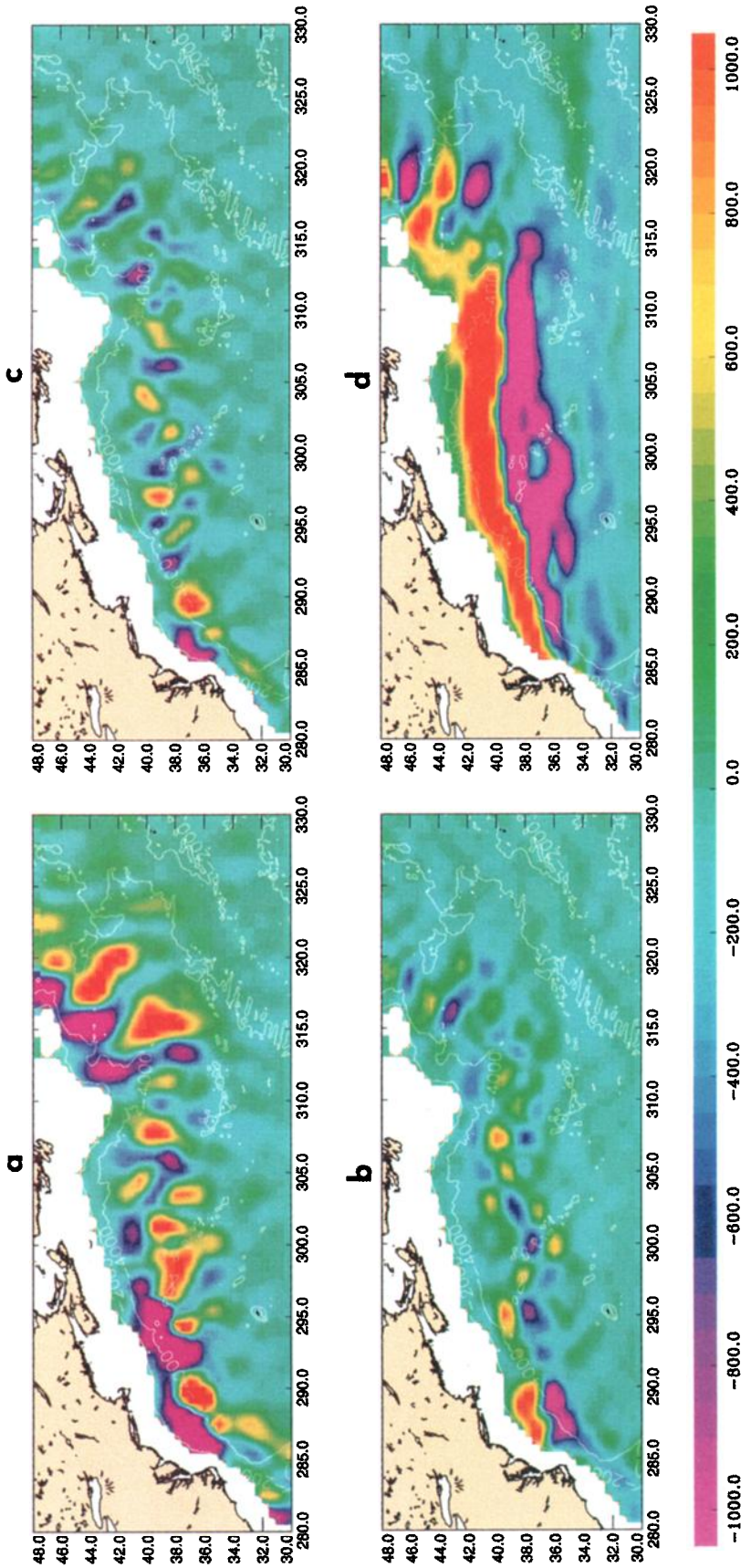

Plate 9. Horizontal eddy momentum flux convergence in the GS. Contributions of (a) $-\langle u'^2\rangle_x$ and (b) $-\langle u'v'\rangle_y$ for the zonal flux and of (c) $-\langle u'v'\rangle_x$ and (d) $-\langle v'^2\rangle_y$ for the meridional flux. One-quarter degree resolution maps from October 1992 to December 1993 and from March 1995 to October 1997 are used. Units are 10^{-8} cm s^{-2}.

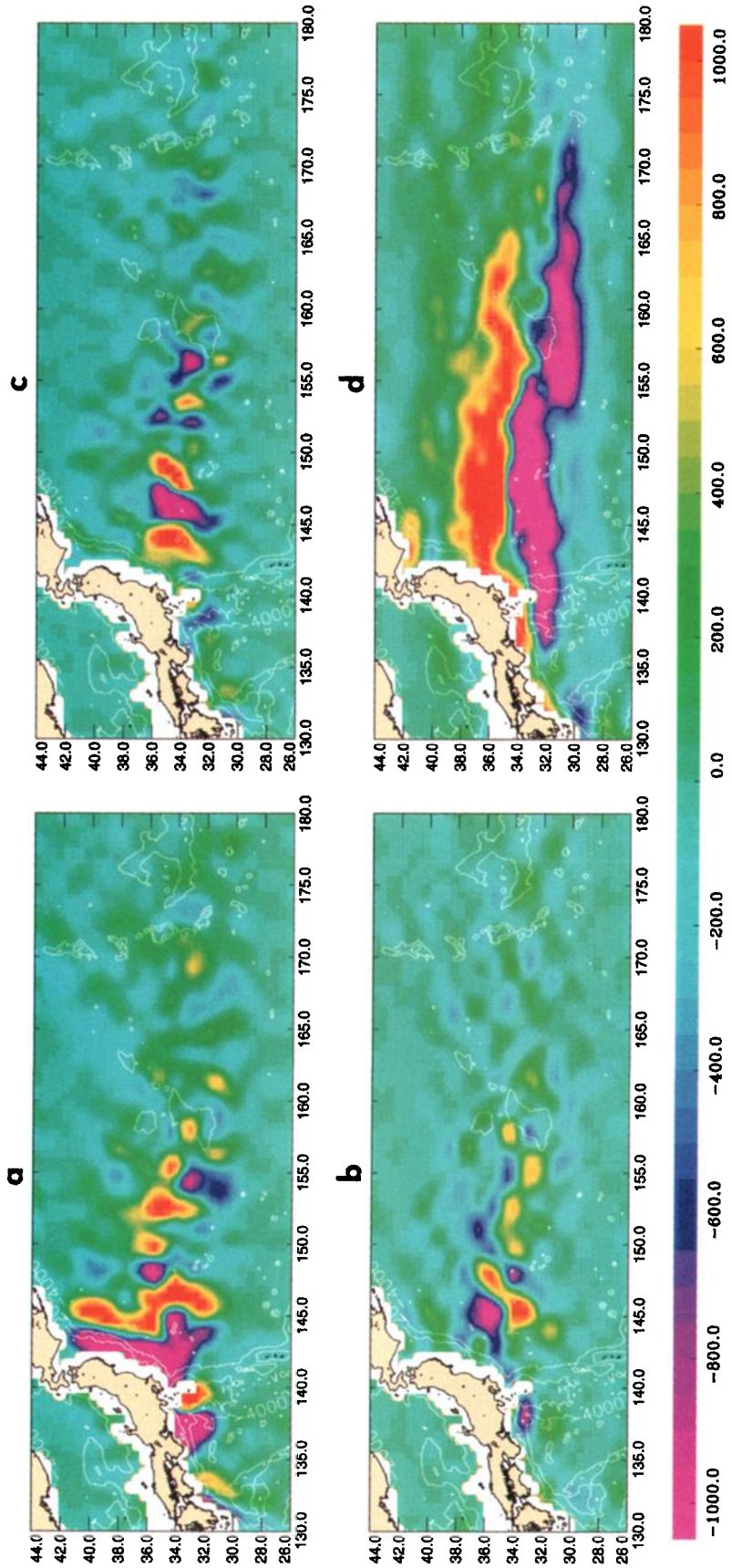

Plate 10. Same as Plate 9 but for the KS.

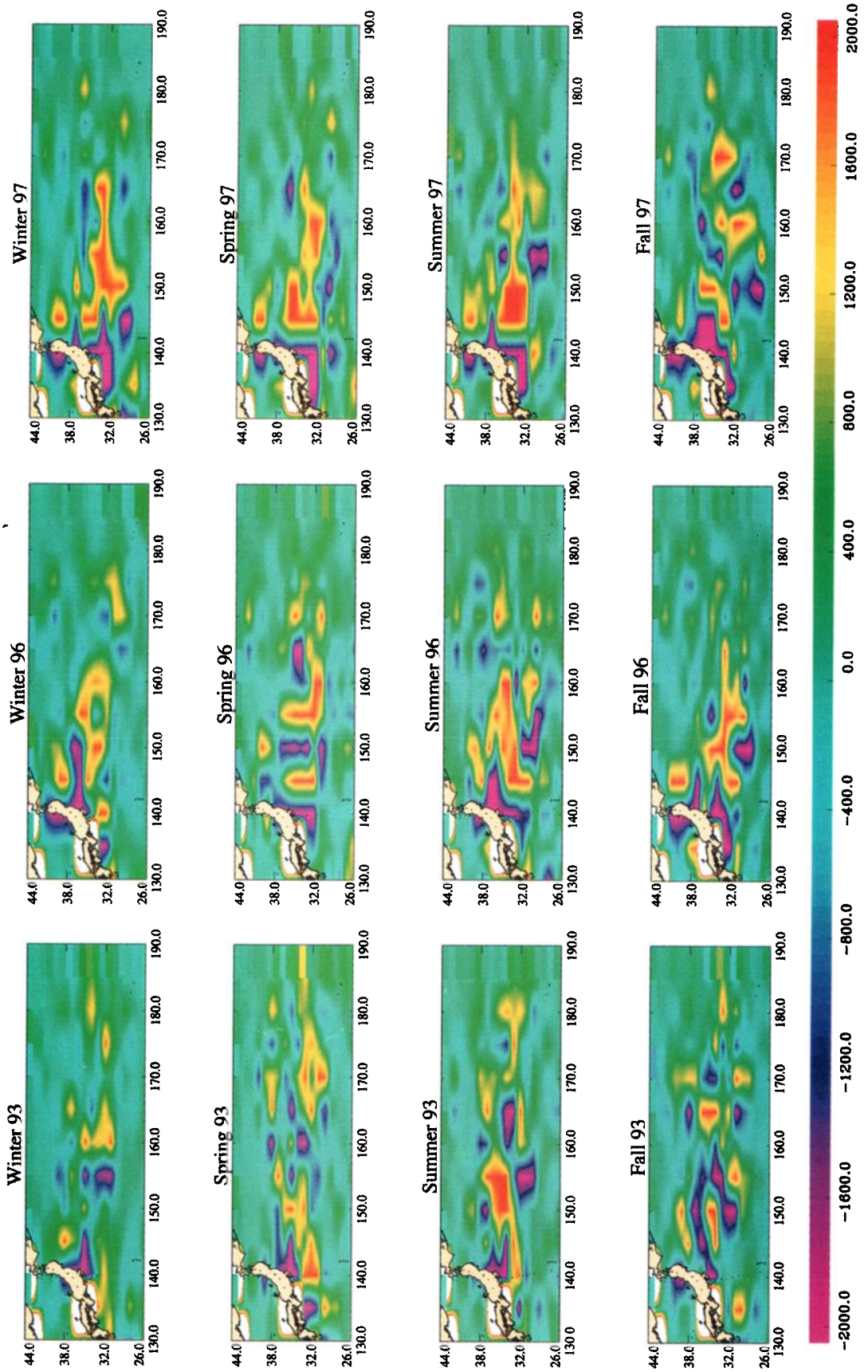

Plate 11. Seasonal means of zonal eddy momentum flux in the KS for years 1993, 1996, and 1997. Winter is the mean of January, February, and March, etc. Maps are averaged in 1° × 5° boxes in latitude and longitude, respectively. Units are 10^{-8} cm s^{-2}.

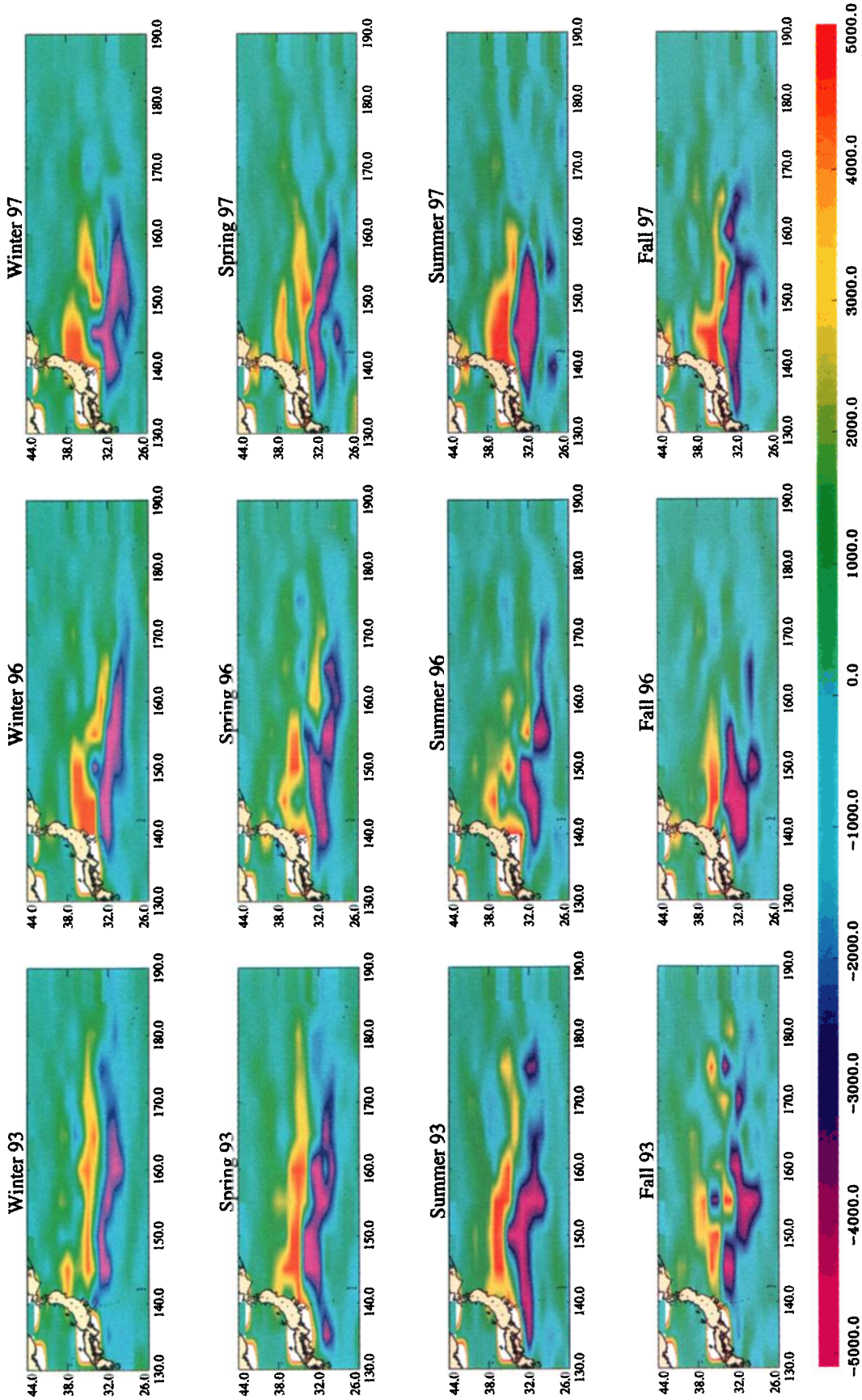

Plate 12. Same as Plate 11 but for seasonal means of meridional eddy momentum flux.

is found in the confluence zone of the fronts of the KS and the Oyashio Currents, where meandering activity is presumably high.

4.1.2. Gulf Stream. As for the KS, the main oceanic features described in section 3 are detailed in Plate 4. As far as seasonal variations are concerned, one might be surprised by the changes in the EKE intensity of the double-blade feature during 1993, maximum in winter/spring and minimum in summer/fall. However, as discussed further in section 4.2.2, these oscillations are not purely seasonal but exhibit semiannual to annual periods, which explains the rather irregular EKE time variations over this area during the following years. Farther east, in the GS Extension, *Shum et al.* [1990] find annual variations in the position of the mean GS, through a descriptive analysis of maximum EKE axis variations. They assert that the path tends to shift northward several degrees in latitude in the summer/fall season and southward by approximately the same distance in winter/spring. We also computed differences of the 3 month averaged EKE from the 5 year mean to assess the seasonal variations, as was done by *Shum et al.* [1990]. Nevertheless, the strong meandering activity along the path of the current that spreads maximum EKE values apart from the mean current axis makes it difficult to establish a clear seasonal signal. Whether a maximum EKE axis can be defined and has a physical meaning and whether it tends to move northward by a few degrees as for the mean axis of the current [see *Kelly*, 1991] is difficult to state.

A signature of the interannual variability is the minimum of EKE generally found around 69°W that disappears in fall 1997 when the zonal extension of the blade structure is also the largest. Also, note the connection with the Florida Current during that season, as well as a strong increase of EKE values in the Florida Current during summer 1997.

Falls 1993 and 1997, as well as winter 1996, clearly show the splitting of the high EKE level path into two branches, east of 64°W, where large meanders can form. The maximum EKE value, of more than 4000 $cm^2\ s^{-2}$ over the 5 year period, is found at 39°N, 64°W, corresponding to the location where *Kelly* [1991] finds the peak in surface transport and also where the width of the stream significantly broadens. As far as the width of high EKE levels is concerned, it can also be seasonally very different (compare, for example, winter 1996 to summer 1997). However, year 1997 does not show any obvious special pattern different from the former years, as in the KS region.

4.2. EKE Monthly Mean Time Series Analysis

By investigating time variations of eddy energy, one expects to gain insight into its sources, [e.g., *Stammer and Böning*, 1996]. In regions of intense currents the main forcing mechanism is generally believed to be instability processes (barotropic and/or baroclinic) of the mean currents [see, e.g., *Qiu*, 1999]. Note that these changes in eddy energy may indirectly result from external surface forcing like wind or buoyancy effects [e.g., *Garnier and Schopp*, 1999]. In a few low eddy variability areas, fluctuating wind stress forcing may play an important role as a direct forcing mechanism in the time evolution of the mesoscale variability [*White and Heywood*, 1995; *Stammer and Wunsch*, 1999].

Because of the lack of about 15 months of ERS 35 day repeat cycle data, we only have 3 complete consecutive years of combined data, which is somewhat short to study EKE seasonal changes. In the Plates 5a and 6, EKE time series are shown from both T/P and T/P + ERS mapped data, the former being useful for the continuity in time of the data series, the latter being complementary by giving a more realistic order of magnitude of the amplitude of the signals. Our goal here is mainly descriptive, referring to and comparing with previous studies. Theoretical discussion is beyond the scope of this paper and should use both altimeter data and high-resolution global circulation modeling results. This work follows the global analysis of the EKE seasonal variations presented by DLTR00. As by DLTR00, EKE monthly values are averaged over 1° by 1° bins and 3 months (the month of March, for example, is the mean of February, March, and April) and computed from November 1992 to May 1998.

4.2.1. Kuroshio and its extension. Plate 5a shows time series of monthly mean EKE, $<u'^2>$, and $<v'^2>$ estimates for T/P only and T/P + ERS maps. Note that the EKE level is systematically significantly underestimated by T/P, by around 30% (see also DLTR00), compared to what we observe with the combined maps. The analysis focuses on the area defined by 130°E–170°W, 26°–44°N, including the KS Current and its extension (Plate 5a). The geographical definition of this region is somewhat arbitrary, and here we follow that of *Wang and Koblinsky* [1995]. Note that the choice of the study area in such a high-variability area can significantly affect the mean level of EKE. However, this point is not relevant in our analysis as we mainly focus on time variations of the mean EKE.

The most striking feature is the significant increase in monthly mean EKE from the beginning of year 1996. During the first 3 years the EKE mean level displays almost seasonal oscillations, regularly peaking in July/August and reaching its minimum in January/February. *Qiu's* [1999] analysis of the EKE time series over the region 30°–40°N, 140°E–170°W from the first 5.25 years of along-track T/P data shows the same variations [see *Qiu*, 1999, Figure 7a]. Nevertheless, Qiu concludes there is no clear annual cycle since the annual/semiannual harmonic curves fitted into the EKE times series explains <25% of the variance in the detrended time series, in contrast with what he finds in the Subtropical Countercurrent (STCC) region (see also DLTR00, Plate 11). This is mainly because he uses the entire time series to fit the harmonics. When looking at Plate 5a, one should separate the full period into two: the first 3 years, showing an almost regular annual cycle that becomes dominated by other frequencies after the end of year 1995.

Qiu et al. [1991], analyzing the first 2.5 years of Geosat Exact Repeat Mission (ERM) data, find annual variations in the SSH differences across the KS, in the upstream region of the flow (west of 154°E), that peak in late September, in agreement with *Zlotnicki's* [1991] results. They also observe that this maximum surface height difference in the KS Extension lags by 2 months the maximum sea level difference at Tokara Strait, upstream of the KS [see also *Kawabe*, 1988]. The region selected in our analysis includes both the KS Current and its extension, which may bias the peak in maximum monthly EKE. In Plate 5 we also plotted the EKE monthly mean time variations in the KS Extension only (as defined by Qiu et al., i.e., 30°–40°N, 140°E–180°) and in the KS Current (30°–35°N, 130°–140°E) from T/P gridded data only. The results correspond to Plates 5b and 5c, respectively. In the KS Current, regular seasonal oscillations, during the first 3 years, can also be observed with some notable points. First, the maximum is found in May, i.e., 2 months before the maximum in the KS Extension, and second, the zonal velocity variance is between 20 and 50% stronger than the meridional one. Interestingly, after 1995

the mean EKE level in the KS Current significantly decreases and remains rather constant till the end of 1998, whereas it keeps increasing in the KS Extension (see below). So, for both the KS Current and the KS Extension the peak values of EKE appear about 2 months before the peak values of the maximum surface transport, which occur in July and September, respectively. To the extent that the maximum surface transport corresponds to the maximum vertical shear, this seems in contradiction with the commonly accepted mechanism of eddy generation through instability processes of mean currents, which would explain a maximum EKE sometime after the maximum in surface transport. However, *Qiu* [1992] shows that the seasonal change in the eastward transport of the KS Current is closely related to the seasonal change in the intensity of the southern recirculation gyre, plausibly forced by local atmospheric forcing. His study also reveals that the southern recirculation gyre intensifies rapidly in winter from January to March, then slows down in the spring months to reach its maximum in July. So, whether the peak of EKE in the KS Current, in May could result from this rapid intensification of the southern recirculation and a resulting associated baroclinic instability remains an open question.

There is a significant drop in the EKE level of 1994, essentially present in the KS Extension area (see Plates 5a and 5b) and to a much lesser extent in the KS Current (Plate 5c). The peak value, during summer, is 20% smaller than for both 1993 and 1995, which was also noted by *Qiu* [1995] and *Adamec* [1998]. *Adamec* [1998] also observes that the normal drop off of the EKE level during winter does not occur in 1995, the minimum of December 1995 being as high as the summer 1994 maximum. *Qiu* [1995] also finds a more or less steady increase of the EKE level in the southern recirculation gyre of the KS Extension from the end of 1992 to mid-1994 and suggests that a likely mechanism to account for this increase is the barotropic instability of the mean flow. Nevertheless, he shows that this process is unlikely to account for the decrease of the EKE level of 1994 within the KS Extension itself. The more recent study of *Adamec* [1998] on the seasonal signal of the EKE of the KS Extension during 1994 focuses on this low EKE event, most apparent during summer and fall 1994, which is also detectable in a measure of the total surface kinetic energy. Basing his analysis on both T/P altimeter and AVHRR sea surface temperature data, he concludes that it is most likely the interaction of the flow field with the thermal field that modulates the seasonal signal of the KS Extension over this time period. During summer 1994 the convergence of heat flux due to eddy flow tends to cool the surface to the south of the KS Extension and to warm the surface to the north, causing a decrease in the large-scale surface baroclinicity across the KS Extension and hence in the surface kinetic energy. During summers 1993 and 1995 the opposite occurs. However, *Adamec* [1998] does not identify any trigger mechanism for these changes in the thermal structure of the current system.

From the beginning of 1996 the regular oscillations are suddenly broken, and the mean EKE keeps increasing till it reaches a first maximum in January 1997 of more than 700 cm^2 s^{-2} (Plate 5b). Interestingly, *Kawabe* [1988] observed that the amplitude of the seasonal cycle of the KS transport was largest during the formation years of the large meander state and in the years immediately preceding an El Niño event. He also found that most of the seasonal variations disappear during the El Niño warm event. The same behavior is found in the EKE variations of the KS Extension, where a sudden drop, at the end of year 1997, leads the mean EKE level back to its value of the end of year 1995. One can then wonder to what extent the EKE level in the KS Extension could result from the surface transport variations of the KS and, with a possible connection to the tropics, if the drop in EKE of the KS Extension during summer 1994 could be related to the rapid succession of warm equatorial events, with 1994 being somewhat warmer than the preceding years [*Adamec*, 1998].

During that period of significantly different behavior of the EKE, between July 1996 and May 1997, the zonal component of the velocity variance is systematically stronger, up to 30% higher in September/October 1996, than its meridional component (see Plate 5a). This suggests that this progressive increase of the EKE level is associated with an acceleration of the mean flow of the KS Extension. A tentative explanation will be presented in section 5, focusing on horizontal eddy processes.

4.2.2. Gulf Stream and its extension. The same analysis is performed in the GS region, defined by 80°–30°W, 28°–48°N. Results are shown in Plate 6. Note that the results presented here are not very sensitive to the geographical area of averaging. Time variations of the monthly EKE do not reveal any clear annual signal during the first 3 years, as in the KS Extension region. Nevertheless, from the beginning of 1995, EKE fluctuations seem to undergo rather regular seasonal oscillations, with a maximum peak in September/October and a minimum found in January/February. Note that this maximum coincides with the maximum of sea level slopes across the current and of surface transport found in previous studies [*Zlotnicky*, 1991]. In Plate 6, $<v'^2>$ is systematically slightly stronger than $<u'^2>$. This is mainly because the selected area contains the northward deflection of the current, around 45°W, where meridional velocities are much stronger than zonal ones. We selected different geographical areas, smaller and closer to the mean current axis (e.g., 35°–41°N, 75°–45°W) which revealed that the monthly mean distribution of both components of the eddy velocity field is almost isotropic, contrary to what was found in the KS Extension area. In that sense the behaviors of the GS and the KS, as far as their eddy energy time variations are concerned, are significantly different. Year 1996 is also, however, an anomalous year, with a maximum energy peak present in September, around 650 cm^2 s^{-2}, at least 20% higher than for the other years. We also extracted the time series of monthly mean EKE over the area defined by 35°–39°N, and 75°–68°W, corresponding to the double-blade structure described in section 3.2 (not shown). The zonal velocity variance is systematically 50% higher than the meridional one, which was somewhat expected. Sixty percent of the total EKE variance is explained by periods between 6 months and about 1.5 year, thus confirming the previous results of *Vazquez et al.* [1990].

4.3. Long-Term Variations

EKE time series can be considered as a measure of long-term fluctuations in the mesoscale variability from direct observations, about which little is known today [*Wang and Koblinsky*, 1999]. An interesting indication on the EKE long-term variability is given in Plate 7, which shows the linear trend of the monthly averaged EKE time series.

The most conspicuous feature in Plate 7 appears in the KS, where a zonal band corresponding to the whole KS Current system exhibits three different areas: the KS Current itself, south of Honshu, with an annual decrease of the mean EKE

level of more than 100 $cm^2\ s^{-2}$; the western part of the KS Extension (from 140° to 155°E), with an annual EKE increase of about 300 $cm^2\ s^{-2}$; and its eastern part (155°E–175°W) showing a negative slope in the EKE time series of up to 150 $cm^2\ s^{-2}\ yr^{-1}$. Over the 5.5 year period this amounts to a 40% increase over the mean EKE level of the western part of the KS Extension and to a 40% decrease in both the KS Current and the eastern part of the KS Extension. A similar analysis was done by *Wang et al.* [1998], who computed a linear trend in the low-pass–filtered sea level change using the first 4.2 years of along-track T/P data. They found a spatial structure of the linear trend basically zonal, with alternating zonal bands of positive and negative trend, which are likely related to what we observe on EKE long-term variations.

No such drastic time variations are observed in the GS. The main notable trend there is seen offshore of Cape Hatteras and shows an annual increase of about 100 $cm^2\ s^{-2}$. These changes again assess the strong differences existing between the time variations of the EKE field in both current systems. Though very significant, the details of the long-term changes in the EKE fields of these current systems will not be discussed further in this work.

5. Eddy/Mean Flow Interactions

This section focuses on the influence of the eddy variability upon the time mean flow through eddy momentum flux convergence and concentrates upon the role that horizontal eddy processes play in accelerating or decelerating the mean flow. Both the spatial averaging and the relative contribution of the different terms of the horizontal eddy momentum flux convergence equations are discussed. A tentative explanation is given for the anomalously large $<u'^2>$ at the end of 1996 in the KS Extension (see 4.2.1).

5.1. Horizontal Eddy Processes

The contribution of the eddy field to the acceleration/deceleration of the mean flow is given by the time-mean momentum equations [see, e.g., *Wang and Koblinsky*, 1995]:

$$-[<u'u'>_x + <u'v'>_y] \quad (1)$$

$$-[<u'v'>_x + <v'v'>_y], \quad (2)$$

where angle brackets represent time averages of the velocity anomalies and (1) and (2) correspond to zonal and meridional horizontal eddy momentum flux convergence, respectively. A positive value of (1) ((2)) tends to accelerate the mean flow zonally (meridionally).

Of the three terms of the horizontal tensor components ($<u'v'>$, $<u'^2>$, and $<v'^2>$) the meridional gradient of the cross-stream term, $<u'v'>_y$, is usually considered to have the most important effect upon the mean momentum balance and is the concern of several studies on eddy/mean flow interactions: *Nishida and White* [1982] (hereinafter referred to as NW82), *Tai and White* [1990] (hereinafter referred to as TW90), and *Adamec* [1998], among others, performed such an analysis. The general pattern of $<u'v'>$ spatial distribution in the KS suggests eddy flux of mean zonal momentum toward the jet; that is, the velocity cross-covariance term is negative north of the axis of the mean flow and positive south of it (NW82 and TW90). As a result, there is a tendency for eastward mean flow intensification. However, NW82 and TW90 are based upon zonally averaged quantities of horizontal eddy processes (NW82 compute mean quantities along a line representing the mean flow axis, west of the Shatsky Rise, slightly oriented northwest-southeast, which still results in a "rotated zonal averaging") owing to a coarse estimation of both components of the geostrophic velocity, whereas one would have rather to follow the jet in order to resolve meanders as done by *Qiu* [1995]. This latter finds the cross-covariance term to be negative on both sides of the KS Extension, from the first 2 years of T/P, whereas TW90 used Geosat data. Whether this discrepancy is due to natural time variability of the momentum flux or to the different averaging technique remains unclear.

The "optimally" combined T/P and ERS data set gives us a chance to get a better estimate of the eddy velocity autocovariance and cross-covariance terms and of their horizontal gradients. From both components of the eddy horizontal velocity we estimate eddy processes in the mean momentum equation balance and compare them in the KS and the GS. We show that (1) zonal averaging is not well adapted to this kind of study and might explain some differences between conclusions of previous analyses and (2) the meridional gradient of $<u'v'>$ is not the term with the largest amplitude in (1), and that to study correctly the interactions of horizontal eddy processes on the mean flow, one has also to compute the zonal gradient of $<u'^2>$.

5.1.1. Influence of spatial averaging on eddy momentum flux convergence. Plate 8 shows the spatial distribution of $<u'v'>$ inferred from the full 0.25° × 0.25° resolution maps for (a) the GS and (b) the KS. Positive and negative values alternate zonally in both current systems. This is particularly obvious in the KS, where such a pattern corresponds to the quasi-stationary meander system. In the GS the differences of flow regimes between the regions west and east of the NESC are well observed: whereas $<u'v'>$ is mainly positive in the former, corresponding to almost zonal mesoscale variability, it shows many zonal changes in the latter region, likely generated by strong meandering activity. From Plates 8a and 8b, zonal averaging is then clearly not adequate to study horizontal eddy processes, which is particularly striking in the case of the KS, even when a priori averaging in 1°×1° boxes is applied to the maps of Plate 8 (not shown). One should rather compute mean quantities following the mean axis of the currents, as done by *Qiu* [1995]. This might explain the difference in the sign of the cross-covariance term of the Reynolds tensor between his results and those of TW90 and NW82. Indeed, no general tendency on the sign of the meridional gradient of $<u'v'>$ can be established from Plate 8. NW82 also found negative values of $<u'v'>$ over the Shatsky Rise, near 160°E, whereas Plate 8 exhibits positive values at that location.

5.1.2. Contribution of the different terms of eddy momentum flux convergence. Plates 9 and 10 show both terms of the zonal (1) and meridional (2) eddy momentum flux convergence in the GS and the KS, respectively. The gradients are calculated by finite differences over three consecutive points and then averaged in 1° by 1° geographical boxes. For the zonal momentum one can observe that $-<u'v'>_y$ is not the predominent term in the zonal eddy momentum flux, but rather $-<u'^2>_x$, which has a stronger amplitude almost everywhere along the path of the currents. Thus *Adamec*'s [1998] discussion about the zonally averaged meridional profiles contribution of the convergence of Reynolds stresses to the zonal momentum budget, $-<u'v'>_y$ to try to explain the large EKE values during fall 1993, may not be complete. The same applies to *Garnier and Schopp* [1999], who assert that as zonal scales

are larger than meridional scales along eastward jets in the ocean, the meridional gradient of cross-covariance velocity dominates the zonal one. Both terms have then to be conserved to study horizontal zonal eddy processes.

The meridional eddy momentum flux is essentially dominated by the meridional gradient of $<v'^2>$, whose pattern deserves attention; nearly zonal sharp gradients suggest the presence of a force that tends to tear the mean flow away from its mean axis, increasing the mean north-south momentum to the north and decreasing it to the south. The intersection between positive and negative gradients is a very well defined thin curve, even without applying any averaging on the maps (not shown), and could then give a rather precise representation of the mean axis of the current (Plates 9d and 10d).

The pattern for the spatial distribution of momentum fluxes and its relative repartition among the different terms is identical in the KS (Plate 10). Alternate meridional bands of positive and negative values are evident in the zonal derivatives of $<u'^2>$ and $<u'v'>$ (Plates 10a and 10c) because of the meandering structure of the current. The meridional gradient of $<v'^2>$ also presents a shape similar to the GS. Note, however, the two almost zero gradient areas separating zonal bands of high amplitudes: at 144°E, 34°N, where a meander of the mean flow takes place, and at 162°E, 34°N, just east of the Shatsky Rise.

As far as the term $-<u'v'>_y$ is concerned, even though it is not the dominant term of the total zonal eddy momentum flux convergence, it can inform us of local tendencies for mean flow acceleration/deceleration. When $-<u'v'>_y$ is positive (negative), it suggests an eastward (westward) acceleration of the mean flow. Westward acceleration is likely associated with recirculating flows in an eastward jet. To the extent that the mean axis is characterized by eastward accelerations one can localize it by following positive values of $-<u'v'>_y$. From Plate 9b, there is a tendency for eastward acceleration between 285°E, 36°N and 298°E, 39°N on a southwest-northeast axis, with a tendency for recirculating mean flow just south of it. In the KS, positive values of the gradient are found along the path of the current, following the meandering pattern; maximum values correspond to crests and troughs of the meanders: at 146°E, 33°N (trough), where both maxima of mean flow intensity and EKE are found (NW82), at 148°E, 36°N (crest), and at 156°E, 32°N, just west of the Shatsky Rise. Possible recirculating flows associated with negative values of the gradient (westward acceleration) are observed at 146°E, north of 35°N, at 148°E, south of 35°N, and from 148°E, 36°N to 156°E, 34°N.

5.2. Seasonal Variations

We now attempt to give an explanation for the singular pattern observed in the KS at the end of 1996 (Plate 5a), where $<u'^2>$ is up to 30% stronger than $<v'^2>$ (see section 4.2.1). The idea is the following: we have seen that the zonal eddy momentum flux acts as an acceleration/deceleration of the mean flow, whereas its meridional counterpart tends to spread it apart from its mean axis. Then, if the former increases and, simultaneously, the latter decreases, one could expect a relatively strong eastward acceleration of the mean flow and a possible enhancement of mesoscale activity generation through instability processes.

We then computed seasonal means of both terms (1) and (2) for years 1993, 1996, and 1997, averaged over 1° latitude × 5° longitude boxes. Maps are shown in Plates 11 and 12 for zonal and meridional momentum fluxes, respectively; whereas there is a general well-established pattern for (2) (Plate 12), which consists of positive values north of the mean axis and negative values to its south, there is not any clear standing feature for (1) (Plate 11). The structure observed for (2), roughly speaking, leads to the conclusion that the eddy variability accelerates the mean flow to the north of about 34°N and decelerates it to the south. There do not seem to be any clear seasonal variations of these quantities. Interestingly, zonal bands of strong meridional fluxes extend farther east in 1993 (up to 180°E) than in the following years. The same pattern was found on the EKE spatial distribution (Plate 3), with high EKE levels and meandering activity extending farther east in 1993 than in 1996 and 1997.

Furthermore, one can observe that summer 1996 seems rather anomalous, in the sense that the zonally well-organized structure generally present in other times is broken. This means that the force that tends to tear the mean flow apart from its axis is expected to be smaller at that period. Similarly, from Plate 11, where clear tendencies on convergence of the zonal momentum cannot be established, there is, however, a well-defined zonally shaped band of high values, extending from about 145° to 165°E, near 34°N, in summer 1996. This structure is associated with an eastward mean flow acceleration and is also present in fall 1996 and winter 1997. Therefore it seems that both a decrease of the meridional eddy momentum flux convergence and an increase of its zonal component take place simultaneously during summer 1996. All we can say at this stage of the discussion is that this situation matches the sudden increase of the zonal component of the velocity variance observed from August 1996 (see Plate 5a). The difference between $<u'^2>$ and $<v'^2>$ is maximum in October 1996 and thus occurs a few months after the situation in summer 1996 for the momentum fluxes. This time lag between the two maxima could then correspond to a characteristic timescale of baroclinic instability [*Adamec*, 1998].

6. Conclusion

Using altimeter data from the first 5.5 years of T/P and ERS-1/2 35 day repeat cycle data, we have shown the contribution of their merging to mesoscale ocean studies in the GS and the KS Current systems, focusing on EKE variations in space and time. A description of the EKE spatial distribution in these two western boundary currents and their extension, based on the 0.25° resolution combined map set, showed some detailed energetic differences between both regions. It indicates that the EKE field is strongly anisotropic all along their respective paths, whether owing to the system of four quasi-stationary meanders along the KS path or to zonal changes on each side of the NESC in the GS. It also assesses the close, even though just visual, relationship between EKE high level spatial distribution and bottom topography. A striking and new ocean feature is found in the GS, shaped as a zonal double-blade structure in the EKE field, centered at 37°N, 71.5°W, which likely corresponds to a regular and permanent lateral displacement of the mean path of the current at this geographical location. Seasonal variations of the EKE spatial distribution were shown in 1993, 1996, and 1997, revealing strong interannual changes in the KS that do not occur in the GS.

Monthly mean EKE time series were analyzed in both current systems. In the KS Extension (30°–40°N, 140°–180°E) the analysis revealed significant changes in the EKE time variations. The well-marked seasonal cycle of the first 3 years

(1993–1995), where the EKE is maximum in July/August, is followed by a constant increase of its level, from the beginning of year 1996 till the beginning of 1997, associated with a suggested zonal acceleration of the eastward flow, $<u'^2>$ being up to 30% higher than $<v'^2>$. EKE seasonal changes were also plotted in the KS Current (30°–35°N, 130°–140°E) and also showed a regular annual cycle during the first 3 years, which precedes by 2 months (maximum in May/June) the EKE seasonal cycle in the KS Extension. EKE oscillations in both regions precede by 2 months the maximum surface transport found by *Qiu et al.* [1991] and *Zlotnicki* [1991]. In the GS region, no such annual cycle is found during the first 3 years, and both zonal and meridional components of the eddy velocity variance remain close to each other. However, rather seasonal oscillations are observed from the beginning of 1995. The maximum EKE occurs in September/October and coincides with the maximum of the surface transport found by *Zlotnicki* [1991]. In both current systems, year 1996 is found to be anomalous, with EKE levels more than 20% higher compared to the other years.

So, at least in the KS and to a lesser extent in the GS, the commonly accepted mechanism of eddy generation through instability processes of mean currents, which would explain a maximum EKE sometime after the maximum in surface transport, is not likely at work (assuming that previous estimates of surface transports are correct). This observed increase of mesocale variability during summer is neither due to seasonally varying wind stress, which would rather explain the inverse seasonal increase of EKE during the cooling season (i.e., fall and winter), as observed in the northeastern Atlantic Ocean. A plausible mechanism was proposed by *Strass et al.* [1992], who suggested that the formation of the seasonal pycnocline in a baroclinic field, by setting up the seasonality of the necessary condition of the baroclinic instability (i.e., the vertical reversal of the isopycnic potential vorticity gradient), leads to a temporal increase of mesocale spatial variability during the heating season (in summer, when the seasonal pycnocline is formed). However, in that case we should find the same seasonal cycles in both regions, which is not the case. Clearly, other physical processes contribute to the mesoscale variability, which will be further investigated.

Drastic long-term EKE changes in the KS were also observed, zonally distributed as a "tripole." A 40% increase of the mean EKE level of the western part of the KS and a 40% decrease in both the KS Current and the eastern part of the KS are observed over the 5.5 year period and are not present in the GS.

Focusing at last on horizontal eddy momentum fluxes, we first showed that one has to be careful when averaging these quantities zonally. In particular, the pattern of the spatial distribution of the Reynolds stress cross-covariance term $<u'v'>$ presents high zonal variations from place to place and is not well adapted to zonal averaging. Second, to study convergence/divergence of the mean flow due these fluxes, one has to take all terms into account and not just the meridional gradient of $<u'v'>$, which is commonly done. Finally, looking at the seasonal variations of the horizontal fluxes of momentum, we gave a tentative explanation for the zonal acceleration observed in the KS at the end of 1996, which could result from the strong convergence of zonal eddy momentum fluxes and a weakening of its meridional counterpart, both being observed simultaneously in summer 1996.

Combined data analyses are being extended to comparisons with high-resolution numerical models. These comparisons are aimed to understand better the forcing mechanisms of the observed mesoscale variability and to characterize the skills of the very high resolution models to simulate accurately these current systems. Recent improvement in accurately stimulating the GS [*Chao et al.*, 1996; *Smith et al.*, 2000] and the KS [*Hurlburt et al.*, 1996; *Mitchell et al.*, 1996] with high-resolution basin-scale primitive equation models enables us to make direct meaningful quantitative comparisons with observations. In that sense the EKE and Reynolds stresses analyses presented here would be a next step to test the capacity of the model to reproduce their seasonal and interannual fluctuations.

Acknowledgments. We are grateful to Gilles Reverdin for his comments on an earlier version of the manuscript. The objective analysis code was run on a Silicon Graphics Power Challenge at European Center for Research and Advanced Training in Scientific Computation (CERFACS), based in Toulouse (France), which allowed us to save much CPU time. This work was realized as part of the Environment and Climate EU AGORA (ENV4-CT9560113) and DUACS (ENV44-T96-0357) projects. The T/P maps and T/P + ERS combined maps that were used in this study are distributed by AVISO on two separate CD-ROMs. This study was partly funded through the DUACS (ENV4-T96-0357) and GANES (ENV4-CT98-0744) projects of the European Union.

References

Adamec, D., Modulation of the seasonal signal of the Kuroshio Extension during 1994 from satellite data, *J. Geophys. Res.*, *103*, 10,209–10,222, 1998.

Chao, S.-Y., Bimodality of the Kuroshio, *J. Phys. Oceanogr.*, *14*, 92–103, 1984.

Chao, S.-Y., A. Gangopadhyay, F. O. Bryan, and W. R. Holland, Modeling the Gulf Stream system: How far from reality?, *Geophys. Res. Lett.*, *23*, 3155–3158, 1996.

Cornillon, P., The effects of the New England Seamounts on Gulf Stream meandering as observed from satellite IR imagery, *J. Phys. Oceanogr.*, *16*, 386–389, 1985.

Ducet, N., P.-Y. Le Traon, and G. Reverdin, Global high resolution of ocean circulation from TOPEX/Poseidon and ERS-1/2, *J. Geophys. Res.*, *105*, 19,477–19,498, 2000.

Garnier, V., and R. Schopp, Wind influence on the mesoscale activity along the Gulf Stream and the North Atlantic currents, *J. Geophys. Res.*, *104*, 18,087–18,110, 1999.

Hall, M. M., Energetics of the Kuroshio Extension at 35°N, 152°E, *J. Phys. Oceanogr.*, *21*, 958–975, 1991.

Hurlburt, H. E., A. J. Wallcraft, W. J. Schmitz Jr., P. J. Hogan, and E. J. Metzger, Dynamics of the Kuroshio/Oyashio current system using eddy-resolving models of the North Pacific Ocean, *J. Geophys. Res.*, *101*, 941–976, 1996.

Kawabe, M., Sea level variations at the Izu Islands and typical stable paths of the Kuroshio, *J. Oceanogr. Soc. Jpn.*, *41*, 307–326, 1985.

Kawabe, M., Variability of the Kuroshio velocity assessed from the sea level difference between Naze and Nishinoomote, *J. Oceanogr. Soc. Jpn.*, *44*, 293–304, 1988.

Kawabe, M., Model study of flow conditions causing the large meander of the Kuroshio south of Japan, *J. Phys. Oceanogr.*, *26*, 2449–2461, 1996.

Kelly, K. A., The meandering Gulf Stream as seen by the Geosat altimeter: Surface transport, position, and velocity variance from 73° to 46°W, *J. Geophys. Res.*, *96*, 16,721–16,738, 1991.

Le Traon, P.-Y., and G. Dibarboure, Mesoscale mapping capabilities of multiple-satellite altimeter missions, *J. Atmos. Oceanic. Technol.*, *16*, 1208–1223, 1999.

Le Traon, P.-Y., and F. Ogor, ERS-1/2 orbit improvement using TOPEX/Poseidon: The 2 cm challenge, *J. Geophys. Res.*, *103*, 8045–8057, 1998.

Mitchell, J. L., W. J. Teague, G. A. Jacobs, and H. E. Hurlburt, Kuroshio Extension dynamics from satellite altimetry and a model simulation, *J. Geophys. Res.*, *101*, 1045–1058, 1996.

Mizuno, K., and W. B. White, Annual and interannual variability in the Kuroshio current system, *J. Phys. Oceanogr., 13*, 1847–1867, 1983.

Nishida, H., and W. B. White, Horizontal eddy fluxes of momentum and kinetic energy in the near-surface of the Kuroshio Extension, *J. Phys. Oceanogr.*, 12, 160–170, 1982.

Pickart, R. S., Interaction of the Gulf Stream and Deep Western Boundary Current where they cross, *J. Geophys. Res., 99*, 25,155–25,164, 1994.

Qiu, B., Recirculation and seasonal change of the Kuroshio from altimetry observations, *J. Geophys. Res., 97*, 17,801–17,811, 1992.

Qiu, B., Variability of the Kuroshio Extension and its recirculation gyre from the first two-year TOPEX data, *J. Phys. Oceanogr., 25*, 1827–1842, 1995.

Qiu, B., Seasonal eddy field modulation of the North Pacific Subtropical Countercurrent: TOPEX/Poseidon observations and theory, *J. Phys. Oceanogr., 29*, 2471–2486, 1999.

Qiu, B., K. A. Kelly, and T. M. Joyce, Mean flow and variability in the Kuroshio Extension from Geosat altimetry data, *J. Geophys. Res., 96*, 18,491–18,507, 1991.

Shum, C. K., R. A. Werner, D. T. Sandwell, B. H. Zhang, R. S. Nerem, and B. D. Tapley, Variations of global mesoscale eddy energy observed from Geosat, *J. Geophys. Res., 95*, 17,865–17,876, 1990.

Smith, R. D., M. E. Maltrud, F. O. Bryan, and M. W. Hecht. Numerical simulation of the North Atlantic Ocean at 1/10°, *J. Phys. Oceanogr., 30*, 1532–1561, 2000.

Stammer, D., and C. Böning, Generation and distribution of mesoscale eddies in the North Atlantic Ocean, *in Warm Water Sphere of the North Atlantic Ocean,* edited by W. Krauss, pp. 159–194, Gebrüder Borntträger, Stuttgart, Germany, 1996.

Stammer, D., and C. Wunsch, Temporal changes in eddy energy of the oceans, *Deep Sea Res., Part II, 46*, 77–108, 1999.

Strass, V. H., H. Leach, and J. D. Woods, On the seasonal development of mesoscale variability: The influence of the seasonal pycnocline formation, *Deep Sea Res., Part A, 39*, 1627–1639, 1992.

Tai, C.-K., and W. B. White, Eddy variability in the Kuroshio Extension as revealed by Geosat altimetry: Energy propagation away from the jet, Reynolds stresses, and seasonal cycle, *J. Phys. Oceanogr., 20*, 1461–1777, 1990.

Tracey, K. L., and D. R. Watts, On Gulf Stream meander characteristics near Cape Hatteras, J. Geophys. Res., 91, 7587–7602, 1986.

Vazquez, J., V. Zlotnicki, and L.-L. Fu, Sea level variabilities in the Gulf Stream between Cape Hatteras and 50°W: A Geosat study, *J. Geophys. Res., 95*, 17,957–17,964, 1990.

Wang, L., and C. J. Koblinsky, Low-frequency variability in regions of the Kuroshio Extension and the Gulf Stream, *J. Geophys. Res., 100*, 18,313–18,331, 1995.

Wang, L., and C. J. Koblinsky, Large change of mesoscale variability in the Kuroshio Extension region during the first 5 years of the TOPEX/Poseidon mission, *Geophys. Res. Lett., 26*, 2243–2246, 1999.

Wang, L., C. J. Koblinsky, and S. Howden, Annual and intra-annual variability in the region of the Kuroshio Extension from TOPEX/Poseidon and Geosat altimetry, *J. Phys. Oceanogr., 28*, 692–711, 1998.

White, M. A., and K. Heywood, Seasonal and interannual changes in the North Atlantic subpolar gyre from Geosat and TOPEX/Poseidon altimetry, J. Geophys. Res., 100, 24,931–24,941, 1995.

Zlotnicki, V., Sea level differences across the Gulf Stream and Kuroshio Extension, *J. Phys. Oceanogr., 21*, 599–609, 1991.

N. Ducet and P.-Y. Le Traon, Space Oceanography Division, CLS, BPI 1101, 8–10 rue Hermes, 31526 Romonville Saint-Agne, France. (nicolas. ducet@cls.fr)

(Received January 7, 2000; revised December 26, 2000; accepted January 10, 2001.)